Plasma density at the current reversal in the STOR-1M tokamak with AC operation

1992 Nucl. Fusion 32 1801

(http://iopscience.iop.org/0029-5515/32/10/I08)

PLASMA DENSITY AT THE CURRENT REVERSAL IN THE STOR-1M TOKAMAK WITH AC OPERATION

O. MITARAI
Department of Electrical Engineering,
Kumamoto Institute of Technology,
Kumamoto,
Japan

A. HIROSE, H.M. SKARSGARD
Department of Physics,
University of Saskatchewan,
Saskatoon, Saskatchewan,
Canada

ABSTRACT. The plasma density behaviour in the STOR-1M tokamak with alternating current (AC) operation is described using the Murakami–Hugill diagram ($1/q_a$, $\bar{n}R/B_t$). At the current reversal, $I_p = 0$ ($1/q_a = 0$), the plasma density remains finite and the Murakami parameter is $\bar{n}R/B_t = (0.66 \pm 0.22) \times 10^{18}$ $m^{-2} \cdot T^{-1}$. Gas puffing before the current reversal does not noticeably increase the plasma density at the current reversal, but allows AC operation with larger currents and improves its reproducibility. A qualitative explanation for the finite plasma density at the current reversal is given on the basis of a short circuit effect by the limiter.

1. INTRODUCTION

Alternating current (AC) operation of a tokamak reactor is an attractive scenario to generate a continuous output of electric energy with a minimum thermal energy storage [1]. A recent study of an AC tokamak reactor revealed the attractiveness of this scenario enhanced by Ohmic ignition and bootstrap current [2]. The first experimental demonstration of AC operation was made in the STOR-1M tokamak [3]. It was found that the plasma density remains finite during the current reversal phase with negligible rotational transform. In AC tokamak reactors, the residual plasma density during the current reversal phase will eliminate the need of preionization at the beginning of successive half-cycles and thus ease the rate of time variation of the current in superconducting Ohmic transformers. At present, little is known about the scaling of the residual density at the current reversal with plasma parameters, such as the major/minor radii, the toroidal magnetic field and the current rampdown rate. Not only will the establishment of an empirical scaling be useful for designing AC tokamak reactors but it may also shed light on the mechanism of plasma confinement with negligible rotational transform.

The objective of this paper is to describe the behaviour of the plasma density near the current reversal in order to provide a database for the scaling of the residual plasma density at the current reversal, and to demonstrate the effect of gas puffing on the plasma density and AC operation. To this end, we employ the Murakami–Hugill diagram [4] in which $1/q_a$ and $\bar{n}R/B_t$ are plotted to trace the temporal behaviour of a tokamak discharge. Usually, the Hugill limit predicts a linearly decreasing relation between the density and the plasma current, $\bar{n}_e \sim I_p$ [5]. For transient discharges, such as in AC operation, this relation no longer holds near the current reversal, and the value of $\bar{n}R/B_t$ can be finite at $1/q_a = 0$, as found in STOR-1M.

A schematic trace of the operating point on the Murakami–Hugill diagram is shown in Fig. 1 for 'ideal' multi-cycle AC operation. Positive and negative $1/q_a$ values correspond to plasma current in the positive and negative directions. The density increases from the origin to the higher density regime, decreases towards the origin along the Hugill limit, but with a finite $\bar{n}R/B_t$ ('AC density limit') at $I_p = 0$, and then increases again in the negative $1/q_a$ direction. When STOR-1M discharges are plotted in the Murakami–Hugill diagram, a behaviour similar to the 'ideal' case is seen. The offset value of $\bar{n}R/B_t$ is relatively insensitive to the plasma current and the neutral density controlled by gas puffing.

This paper is organized as follows. Section 2 gives discharge wave forms with gas puffing observed in STOR-1M. Section 3 presents the discharge behaviour and the $\bar{n}R/B_t$ value near and at $1/q_a = 0$ on the

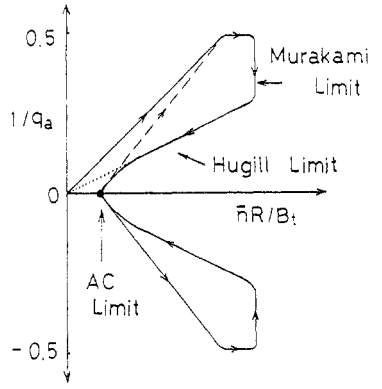

FIG. 1. Schematic trace of the density on the Murakami-Hugill diagram for AC operation.

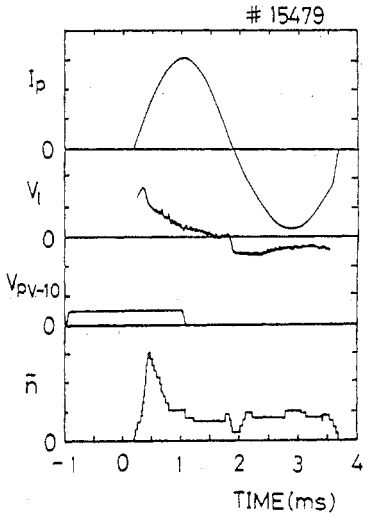

FIG. 2. Temporal evolution of an AC discharge (shot #15479) in STOR-1M with gas puffing. The plasma current rampdown rate is 6.5 kA/ms before the current reversal. The plasma current I_p = 1.31 kA/div, the loop voltage V_ℓ = 10 V/div, $V_{PV\text{-}10}$ is the voltage pulse applied to the PV-10 piezoelectric valve used for gas puffing, and the line averaged electron density $\bar{n} = 2 \times 10^{18}$ m^{-3}/step.

Murakami-Hugill diagram. Section 4 discusses effects of the stray field on smooth AC operation. Section 5 gives a simple formula for the finite density at the current reversal. Section 6 presents a simple model of the particle confinement during the transition from a rotational transform to a current-free confinement. Section 7 gives a discussion and a summary.

2. AC OPERATION WITH GAS PUFFING

Experiments have been performed on the STOR-1M tokamak with a major radius R = 0.22 m, a minor radius a = 0.035 m and a toroidal field $B_t \leq 1$ T. Details of the device are given in Ref. [6]. The plasma current wave forms available in STOR-1M are a normal tokamak discharge, a full cycle AC discharge and a tokamak discharge supplemented by turbulent heating [7]. We discuss here AC discharges of a 4 ms period.

In AC operation, the current producing the vertical magnetic field is also made AC and has a wave form similar to that of the discharge current. The vertical field at the current reversal must be minimized, including the stray vertical field, to achieve smooth current reversal without large voltage spikes. The wave forms for a typical AC discharge are shown in Fig. 2. The peak plasma current is 4 kA in the first half-cycle. Gas puffing is used to control the plasma density, as indicated by the puffer voltage pulse $V_{PV\text{-}10}$. The electron density is maintained at $(7 \pm 1) \times 10^{18}$ m^{-3} before the reversal, drops to $(3 \pm 1) \times 10^{18}$ m^{-3} at the reversal, and then increases again during the phase of negative plasma current rise. The electron density at the instant of the current reversal is relatively insensitive to gas puffing. However, the density in the second half-cycle

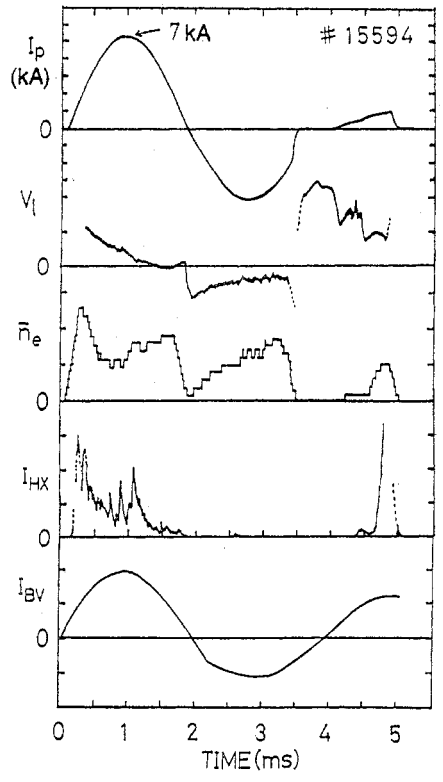

FIG. 3. Temporal evolution of an AC discharge with a large peak plasma current (7 kA) (shot #15594) in STOR-1M with gas puffing. The vertical scales are the same as in Fig. 2. I_{HX} indicates the hard X-ray signal measured by a plastic scintillator placed at one side near the limiter. I_{BV} is the current wave form of the vertical field.

(reverse plasma current) increases with gas puffing. It is to be noted that the resolution in the density measurement is one-quarter fringe, i.e. 2×10^{18} m^{-3}, and we have assumed that there is no change in the minor plasma radius because of plasma shrinkage in the current rampdown phase.

Figure 3 shows the temporal evolution of an AC discharge with a peak plasma current of 7 kA, where the current rampdown rate is about 11.4 kA/ms. The third half-cycle of the plasma current is seen to be incompletely produced, with a time delay of 0.5 ms after disruption of the second half-cycle, because the vertical equilibrium field is not controlled by a feedback system and the horizontal compensation field is not optimized around the second current reversal. While for the first plasma half-cycle the high frequency preionization system (~ 10 MHz) is usually needed to give a reliable breakdown in this small tokamak, the third plasma half-cycle is produced by a breakdown voltage of 25 V without any preionization system. The hard X-ray signal measured by a plastic scintillator placed ~ 1.5 m from the limiter position is also shown. It should be noted that AC operation at a current higher than 6 kA is now reproducibly created with gas puffing.

The residual electron density at the current reversal is thus found to be constant for varying current rampdown rates above 6.5 kA/ms, within the resolution of the density measurement in these experiments. However, the residual density decreases with current rampdown rates below 1.5 kA/ms [3]. It should be noted that while higher plasma current operation (over ~ 6.2 kA) has never been obtained without gas puffing [3], AC operation up to 8 kA has been reproducibly achieved with the help of gas puffing, as shown here.

3. MURAKAMI-HUGILL DIAGRAM FOR AC OPERATION

The Murakami-Hugill diagram corresponding to the discharge with gas puffing (Fig. 2) is shown in Fig. 4(a) near the current reversal phase with $I_p < \pm 1$ kA and a current rampdown rate of 6.5 kA/ms. Here, the relation $1/q_a = (\mu_0 R/2\pi a^2 B_t) I_p$ is used, and the plasma current profile is assumed to have no reverse current layer. As the plasma current decreases, the $\bar{n}R/B_t$ value also decreases to a residual electron density of $\bar{n}R/B_t = (0.66 \pm 0.22) \times 10^{18}$ m$^{-2}\cdot$T^{-1} at $I_p = 0$ ($1/q_a = 0$). Subsequently, the density increases with the current in the negative direction.

Figure 4(b) shows discharges without gas puffing before the current reversal. Four typical shots are

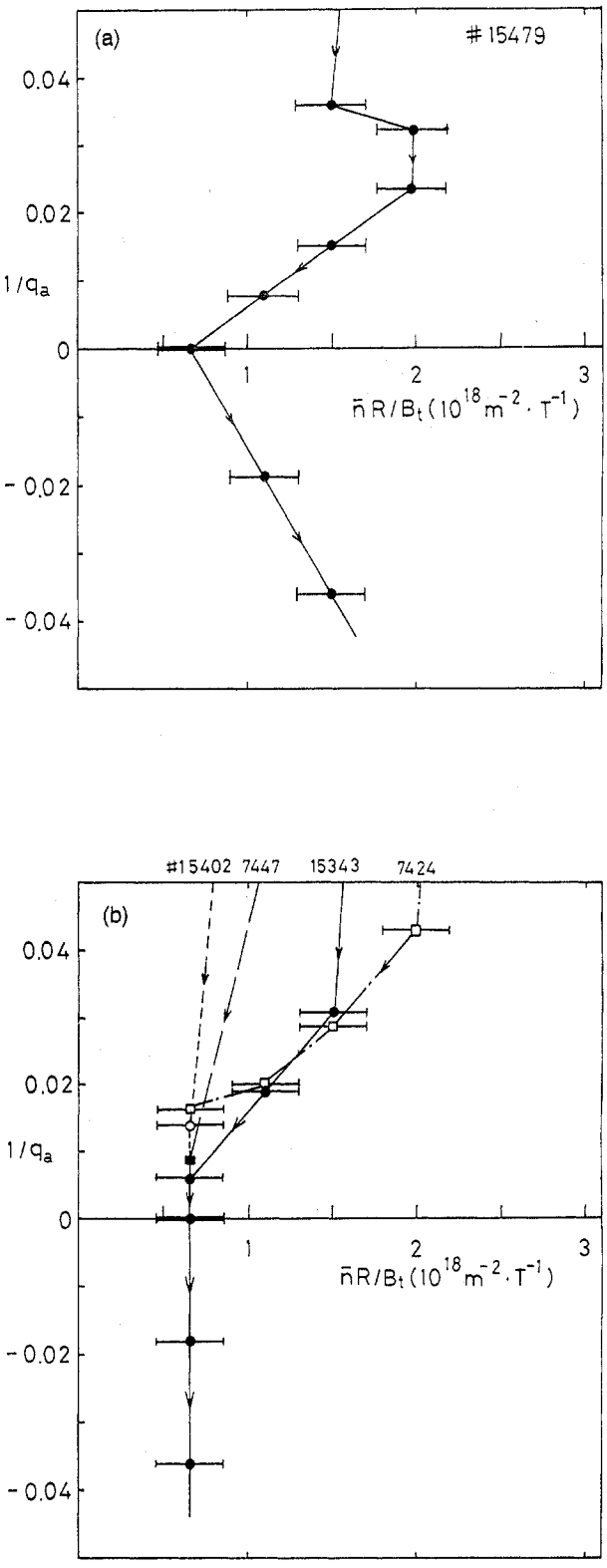

FIG. 4. Density behaviour near $1/q_a = 0$ in the Murakami-Hugill diagram, for AC operation, (a) with gas puffing (data are taken from Fig. 2, shot #15479), and (b) without gas puffing for four shots. The peak plasma current is 4 kA and the current rampdown rate is 6.5 kA/ms for all cases.

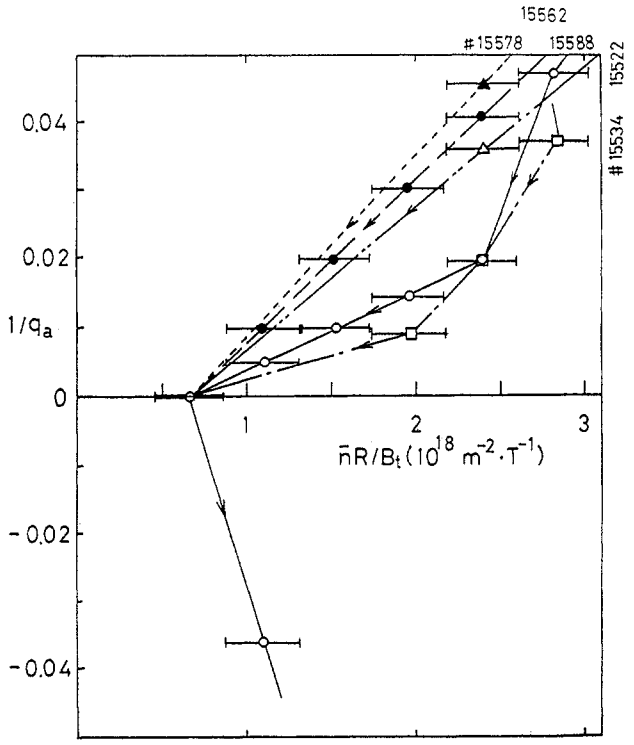

FIG. 5. Density behaviour near $1/q_a = 0$ in the Murakami–Hugill diagram, for AC operation with gas puffing and with a higher plasma current of 6.0–7.6 kA. The peak plasma current and the current rampdown rate are: 6 kA and 10 kA/ms for shots #15522 and #15534, 6.6 kA and 10.9 kA/ms for shot #15588, 7 kA and 11.4 kA/ms for shot #15562, and 7.6 kA and 13.1 kA/ms for shot #15578, respectively.

shown in which the peak plasma current is 4 kA and the current rampdown rate is 6.5 kA/ms, as in Fig. 4(a). In these discharges a higher density corresponds to a higher filling pressure. The $\bar{n}R/B_t$ value just before current reversal is lower than that in the case with gas puffing. However, the $\bar{n}R/B_t$ values at $1/q_a = 0$ are the same for the two cases, within the error bar.

Figure 5 shows similar plots for five typical shots with a higher plasma current of 6–7.6 kA and with gas puffing, where the current rampdown rates are 10.0–13.1 kA/ms. There appears to be little correlation in these data between the density decay rate before the current reversal and the current rampdown rate. The density at the current reversal is still in the same range as in the 4 kA case.

4. STRAY FIELD EFFECT ON AC OPERATION

Smooth AC operation depends on the stray field at the current reversal. In this experiment, an almost time independent horizontal field is provided by the horizontal compensation coil, and the peak vertical equilibrium field is changed to determine the optimum regime of AC operation. Gas puffing is not applied in this experiment.

Figure 6(a) shows the plasma current wave form for the case of a smaller than optimal vertical field. The

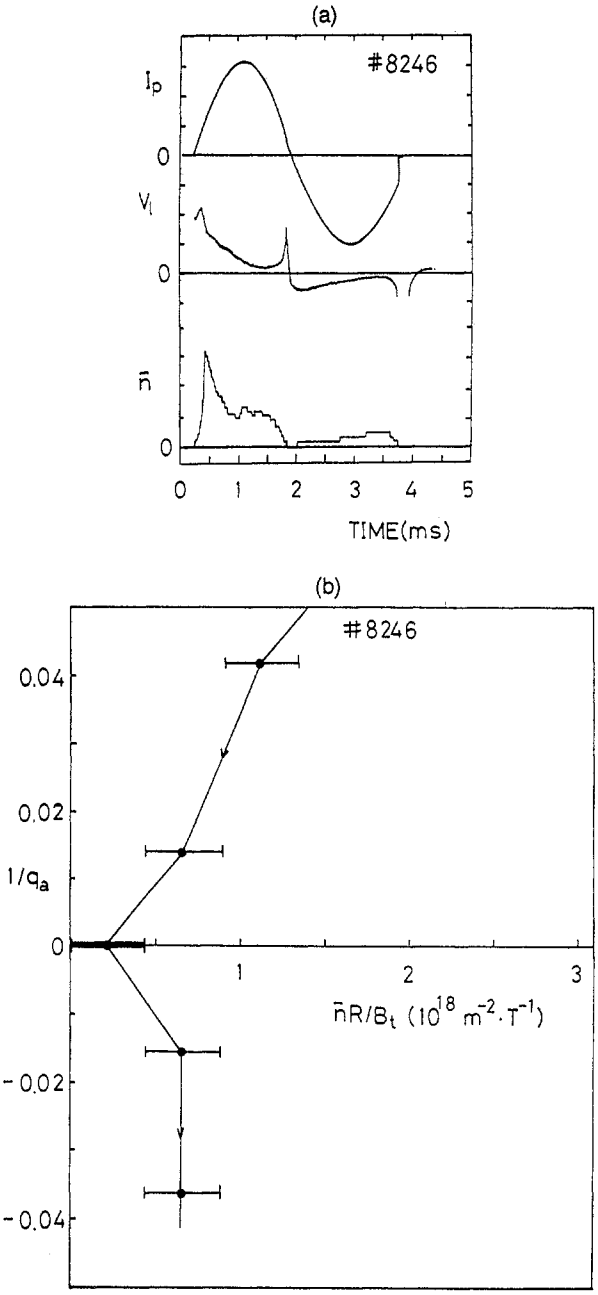

FIG. 6. (a) Temporal evolution of an AC discharge with a positive spike on the one-turn loop voltage, due to a smaller vertical field than the optimal one. (b) Corresponding Murakami–Hugill diagram. Gas puffing is not applied in this case.

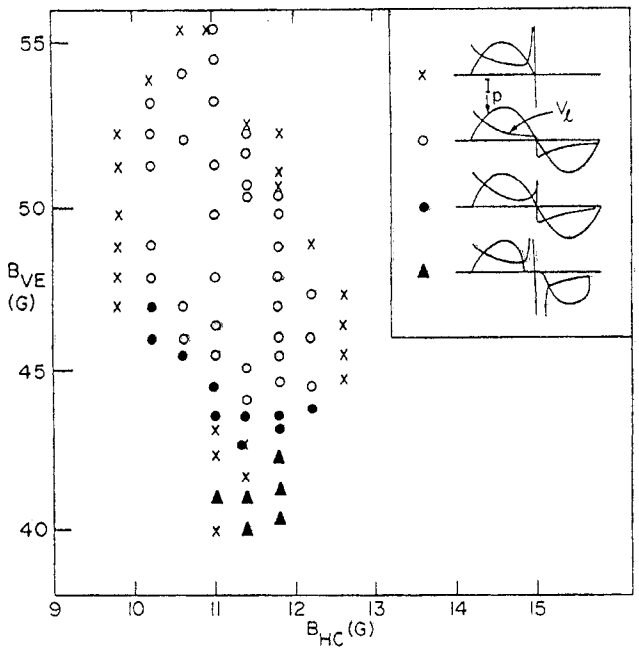

FIG. 7. Optimal regime for smooth AC operation in terms of the horizontal compensation field B_{HC} at the current reversal and the vertical equilibrium field B_{VE} at the peak of the plasma current. Gas puffing is not applied in this case.

plasma current disrupts slightly and the loop voltage shows a positive spike at the current reversal, where the plasma density is decreased to the zero level, within the resolution, during and after the current reversal. On the Murakami-Hugill diagram with the voltage spike at the current reversal, the density decreases to $\bar{n}R/B_t \sim (0.22 \pm 0.22) \times 10^{18}\ m^{-2} \cdot T^{-1}$ at $I_p = 0$, as shown in Fig. 6(b). The small deviation in the vertical field from the optimal value does not, however, affect the overall AC operation.

Figure 7 illustrates the regimes for smooth AC operation, incomplete AC operation and no AC operation in terms of the horizontal compensation field B_{HC} at the current reversal and the vertical equilibrium field B_{VE} at the peak plasma current. The various plasma current wave forms are presented. The optimal peak vertical equilibrium field in the first half-cycle is $B_{VE} \sim 48.8$ G for $I_p \sim 4$ kA. For this vertical field, the allowable horizontal field for complete AC operation is in the range 10–12.2 G, which is quite narrow. When the horizontal compensation field is increased up to 12.6 G, AC operation suddenly becomes impossible; no transitional regime has been observed, unlike in the case of vertical field scanning, indicated by the solid circles. This shows how critically important it is to control the vertical plasma position with an appropriate horizontal field at the current reversal in order to have smooth AC operation. This figure also shows the sensitivity of AC operation to the horizontal plasma position by controlling the vertical equilibrium field near the current reversal.

5. FINITE PLASMA DENSITY AND PARTICLE CONFINEMENT TIME AT THE CURRENT REVERSAL

When the vertical equilibrium field and the horizontal field are carefully optimized, a measurable plasma density remains at the current reversal. This can occur when the particle confinement time is finite at the current reversal owing to the short circuit effect of the limiter, for example [3, 8–11].

When the plasma current is ramped down, the particle confinement time $\tau_{p,rot}$, determined by the rotational transform, is decreased to zero, as given by

$$\tau_{p,rot} \sim a^2/(5.8 D_{rot}) \sim a^2/(5.8 q_a^2 \rho_e^2 \nu_{ei}) \sim I_p^2 T_e^{0.5}/n_e$$

where D_{rot} is the diffusion coefficient derived from the Pfirsch–Schlüter current, ρ_e is the electron Larmor radius with respect to the toroidal field, ν_{ei} is the electron–ion collision frequency and q_a is the safety factor at the plasma edge. This is due to the fact that the vertical electric field E_z, induced by charge separation, increases with a reduction in the rotational transform. However, when the electric field becomes large enough, a short circuit current may flow in the poloidal direction through the limiter and the vacuum chamber, reducing the vertical electric field and the resultant $\vec{E} \times \vec{B}$ radial drift velocity. Thus, the total confinement time can be obtained as the sum of the confinement time due to the rotational transform and that due to the limiter as $\tau_p \sim a/(E_z'/B_t) \sim \tau_{p,rot} + \tau_{p,lim}$. Here the particle confinement time is simply determined by the $\vec{E}' \times \vec{B}$ drift over the plasma radius, where $\vec{E}'$ is the vertical electric field determined by the parallel circuit, as given in Section 6 (Fig. 9(b)). As a result, the confinement time τ_p smoothly approaches the finite value $\tau_{p,lim}$ when the plasma current is reduced to zero. Thus, the plasma density can be maintained at the current reversal.

The behaviour of the electron density at the current reversal should be considered with the help of the power balance and particle balance equation. However, in this paper, we simply estimate the residual density by the particle balance equation:

$$\frac{dn}{dt} = n n_0 \langle \sigma v \rangle_{ion} - \frac{n}{\tau_p} \qquad (1)$$

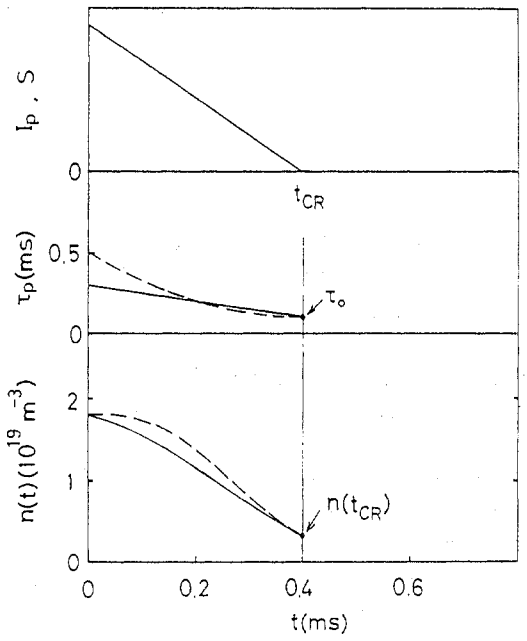

FIG. 8. Temporal behaviour of the plasma current I_p, the density source term $S = nn_0 \langle\sigma v\rangle_{ion}$, the assumed particle confinement time τ_p and the density calculated from Eqs (2) and (3) during the current rampdown phase $t \leq t_{CR}$. The solid lines correspond to Case 1 and the dashed lines correspond to Case 2.

where $\langle\sigma v\rangle_{ion}$ is the ionization rate for hydrogen [12], n_0 is the neutral density and τ_p is the particle confinement time. As the plasma current decreases, the electron temperature also diminishes together with the Ohmic heating power, and the density source term is also reduced through the ionization rate $\langle\sigma v\rangle_{ion}$. Below $T_e \sim 20$ eV, $\langle\sigma v\rangle_{ion}$ decreases almost linearly to zero with the electron temperature. This equation shows, however, that even when the first term becomes zero, the density can remain finite if the particle confinement time τ_p is finite. The density is delayed with respect to the density source term as a consequence of the second term n/τ_p.

For a further examination of the residual density, we assume a linear fall-off for the density source term with $S = nn_0 \langle\sigma v\rangle_{ion} = -n(t - t_{CR})/t_{CR}^2$. We also assume two types of particle confinement time in Eq. (1): *Case 1:* $\tau_p = -\beta(t - t_{CR}) + \tau_0$, with $\beta = -(\tau_1 - \tau_0)/t_{CR}$; and *Case 2:* $\tau_p = -\beta(t - t_{CR})^2 + \tau_0$, with $\beta = (\tau_1 - \tau_0)/t_{CR}^2$, where τ_1 is the confinement time at $t = 0$, τ_0 is the confinement time at the current reversal, and t_{CR} is the current reversal time, as shown in Fig. 8. The second case corresponds to the behaviour $\tau_{p,rot} \propto I_p^2$, as discussed above for a linear current decay. We obtain the density variation after integrating Eq. (1):

Case 1:

$$n(t) = n(0) \exp\left\{\frac{-(t - 2t_{CR})\,t}{2t_{CR}^2}\right\}\left[\frac{-\beta(t - t_{CR}) + \tau_0}{\tau_1}\right]^{\frac{1}{\beta}} \quad (2)$$

Case 2:

$$n(t) = n(0) \exp\left\{\frac{-(t - 2t_{CR})\,t}{2t_{CR}^2}\right\} \times \exp\left\{-\frac{\tan^{-1}\left[\sqrt{\frac{\beta}{\tau_0}}(t - t_{CR})\right] + \tan^{-1}\left[\sqrt{\frac{\beta}{\tau_0}}\,t_{CR}\right]}{\sqrt{\beta\tau_0}}\right\} \quad (3)$$

where n(0) is the density at $t = 0$. Equations (2) and (3) at the current reversal $t = t_{CR}$ become:

Case 1:

$$n(t_{CR}) = n(0) \exp\left\{\frac{1}{2}\right\}\left[\frac{\tau_0}{\tau_1}\right]^{\frac{t_{CR}}{\tau_1 - \tau_0}} \quad (4)$$

Case 2:

$$n(t_{CR}) = n(0) \exp\left\{\frac{1}{2}\right\} \times \exp\left\{-\frac{t_{CR}}{\sqrt{(\tau_1 - \tau_0)\,\tau_0}} \tan^{-1}\left[\sqrt{\frac{\tau_1 - \tau_0}{\tau_0}}\right]\right\} \quad (5)$$

respectively. The density at the current reversal $n(t_{CR})$ is thus found to be finite in both cases for a finite particle confinement time at the current reversal τ_0. This residual density $n(t_{CR})$ increases as expected if the particle confinement times τ_1 and τ_0 increase, and decreases if the current reversal time t_{CR} becomes longer. The latter phenomenon has been observed in the previous STOR-1M experiments (see Fig. 3 in Ref. [3]), where the density at the current reversal decreases as the current rampdown rate dI_p/dt becomes small (large t_{CR}). The behaviour calculated from Eqs (2) and (3) is also plotted in Fig. 8 for the case shown in Fig. 3 of the present paper, with the parameters $n(0) = 1.8 \times 10^{19}$ m^{-3}, $t_{CR} = 0.4$ ms, $\tau_0 \sim 100$ μs (the limiter confinement time described in Section 7), $\tau_1 \sim 0.3$ ms for Case 1 and $\tau_1 \sim 0.5$ ms for Case 2. With these parameters, the density current reversal becomes $n(t_{CR}) \sim 3 \times 10^{18}$ m^{-3}, as observed in these experiments.

6. PARALLEL CIRCUIT MODEL FOR THE CONFINEMENT TIME DURING THE CURRENT REVERSAL

The confinement time during the transition from rotational transform confinement to limiter confinement, $\tau_p \sim \tau_{p,rot} + \tau_{p,lim}$, can be roughly estimated without a detailed discussion of the limiter short-circuit.

The charge balance equation in (r,θ,z) co-ordinates as shown in Fig. 9(a):

$$-\frac{\partial \rho}{\partial t} = \operatorname{div} \vec{J} = \frac{1}{r}\frac{\partial (J_\theta + J_{lim})}{\partial \theta} + \frac{\partial (-J_{d,z})}{\partial z} = 0 \tag{6}$$

provides the vertical electric field as

$$E_z' = \frac{\left(\frac{\partial J_{d,z}}{\partial z}\right)}{\frac{1}{r}\left\{\frac{\partial \sigma_{rot}}{\partial \theta} + \frac{\partial \sigma_{lim}}{\partial \theta}\right\}} \tag{7}$$

Here, the poloidal component of the current density along the twisted magnetic field line is given by $J_\theta = \sigma_{rot} E_z'$, and the current density through the poloidal metal limiter is given by $J_{lim} = \sigma_{lim} E_z'$, where σ_{rot} is the poloidal component of the effective conductivity of the circuit along the twisted magnetic field line and σ_{lim} is the effective limiter conductivity including the sheath region; σ_{rot} is given by $\sigma_{rot} = \sigma_\parallel (B_\theta/B_t)^2 \sin\theta$ in terms of the parallel plasma conductivity $\sigma_\parallel = e^2 n/m\nu_{ei}$, the poloidal magnetic field B_θ and the toroidal magnetic field B_t. $J_{d,z}$ is the charge separation current in the z direction due to the toroidal drift, given by $J_{d,z} = 2n(T_i + T_e)/B_t R$. We see that the denominator in relation (7) for E_z' corresponds to the divergence of the parallel resistances composed of the magnetic field line ($\sigma_{rot} = 1/\eta_{rot}$) and the limiter short-circuit ($\sigma_{lim} = 1/\eta_{lim}$), as shown in the equivalent closed circuit in Fig. 9(b). Using the definition of the independent confinement time due to the rotational transform alone for $\sigma_{lim} = 1/\eta_{lim} \to 0$, i.e. the neoclassical confinement time,

$$\tau_{p,rot} = \frac{aB_t}{E_z} = \frac{aB_t}{r}\frac{\left(\frac{\partial \sigma_{rot}}{\partial \theta}\right)}{\left(\frac{\partial J_{d,z}}{\partial z}\right)} \sim \frac{a}{4R}\left\{\frac{a^2}{q_a^2 \rho_e^2 \nu_{ei}}\right\} \tag{8}$$

and that due to the limiter alone for $\sigma_{rot} = 1/\eta_{rot} \to 0$,

$$\tau_{p,lim} = \frac{aB_t}{E_z} = \frac{aB_t}{r}\frac{\left(\frac{\partial \sigma_{lim}}{\partial \theta}\right)}{\left(\frac{\partial J_{d,z}}{\partial z}\right)} \tag{9}$$

we obtain the total confinement time as

$$\tau_p = \frac{aB_t}{E_z'} = \frac{aB_t}{r}\frac{\left\{\frac{\partial \sigma_{rot}}{\partial \theta} + \frac{\partial \sigma_{lim}}{\partial \theta}\right\}}{\left(\frac{\partial J_{d,z}}{\partial z}\right)} = \tau_{p,rot} + \tau_{p,lim} \tag{10}$$

The limiter confinement time $\tau_{p,lim}$ can be separately estimated from probe theory taking the sheath region into account [11], as described in the next section.

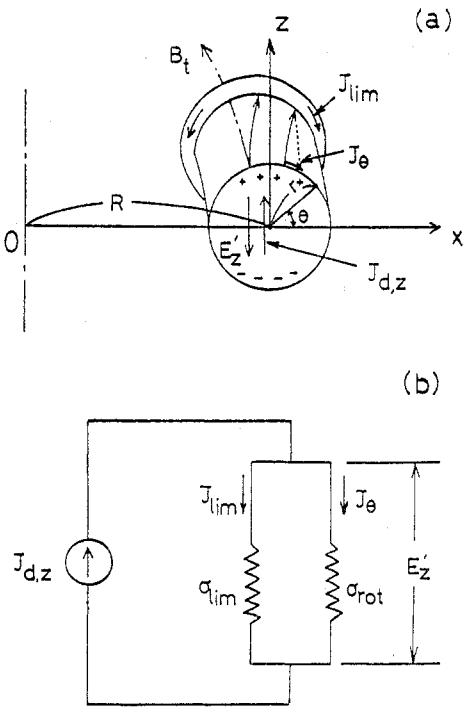

FIG. 9. (a) Schematic drawing of the limiter and the twisted magnetic field lines in the (r,θ,z) co-ordinate. (b) Parallel resistance circuit model for the total confinement time. The closed current is driven by the charge separation.

7. DISCUSSION AND SUMMARY

In order to see whether the finite residual plasma density at the current reversal is an effect peculiar to the small size of STOR-1M, experiments with soft current termination of Ohmic discharges have been performed on a larger tokamak, STOR-M, with a major radius R = 0.46 m, a minor radius a = 0.12 m,

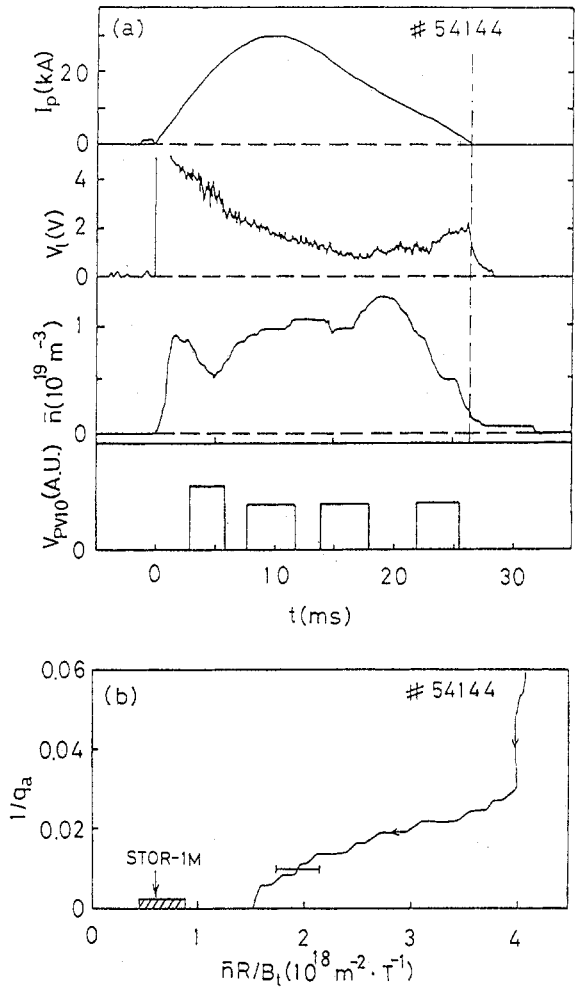

FIG. 10. (a) Temporal evolution of discharges with soft current termination in STOR-M. (b) Density behaviour in the current rampdown phase of Fig. 10(a) for I_p < 5 kA in the Murakami–Hugill diagram. V_{PV-10} is the voltage pulse for gas puffing.

$B_t \sim 0.7$ T and $I_p \sim 28$ kA. In the experiments, as shown in Fig. 10(a), the plasma current is decreased to zero without disruption, at a rate $dI_p/dt \sim -1.5$ kA/ms. As in STOR-1M, a residual density of $\sim 1.8 \times 10^{18}$ m^{-3} has been observed at $I_p = 0$, and it then decays with a time constant of several milliseconds. In terms of the Murakami parameter, $\bar{n}R/B_t \sim 1.43 \times 10^{18}$ $m^{-2}\cdot T^{-1}$ has been obtained at $I_p = 0$, as shown in Fig. 10(b). This is approximately a factor of two larger than in STOR-1M. This type of representation may provide some measure of the density at the current reversal in AC operation. More detailed results will be described in a separate paper [13].

Ion–neutral collisions in a weakly ionized plasma can be expected to suppress the vertical electric field induced by charge separation. This mechanism has been proposed to explain the long lasting decaying plasma in a glass torus without a metal limiter [14–16]. In the current reversal phase, the plasma temperature is reduced and the density is low, while the neutral density is increased by gas puffing. Therefore, it is of interest to see whether this mechanism in a weakly ionized plasma can account for the confinement where there is no rotational transform. The confinement time is given by

$$\tau_{p,in} \sim a/(E_z/B_t) = \{aMR/4\,(T_e + T_i)\}\,\nu_{in}$$

where M is the ion mass, ν_{in} is the ion–neutral collision frequency ($\nu_{in} = n_0\sigma_{in}v_i$), n_0 is the neutral density, σ_{in} is the momentum transfer collision cross-section of the ion with neutral hydrogen and v_i is the ion thermal velocity [15, 16]. In this formula, the vertical drift velocity is compensated by the anti-drift motion of the ions induced by ion–neutral collisions. For the parameters of STOR-1M, with the neutral density $n_0 \sim 10^{19}$ m^{-3} necessary for obtaining the second half-cycle, $\sigma_{in} \sim \pi(1.36 \times 10^{-10})^2$ m^2, and $v_i \sim 1.38 \times 10^4$ m/s for $T_i = 1$ eV, the ion neutral collision frequency is $\nu_{in} \sim 8 \times 10^3$ s^{-1}, and the resultant particle confinement time is only $\tau_{p,in} \sim 0.12$ μs. This value is two orders of magnitude lower than the value of the particle confinement time of ~20–150 μs, which is obtained from the measured density decay rate just before the current reversal, using the approximate relationship $\Delta n/\Delta t \sim -n/\tau_p$ in Eq. (4.1). Therefore, this mechanism does not play a role for confinement at the current reversal.

The confinement time due to the limiter is given by $\tau_{p,lim} \sim a^2 B_t/(T_e U_e)$, with $U_e \sim \{1 - (a/R)^2\}$ using probe theory [11], according to which the limiter current should be smaller than the ion saturation current. The limiter confinement time is $\tau_{p,lim} \sim 126$ μs for the STOR-1M parameters a = 0.035 m, R = 0.22 m, $B_t = 1$ T and $T_e \sim 10$ eV; this is comparable to the measured confinement time of ~20–150 μs mentioned before. It is interesting to note that this confinement time increases as the current reversal is approached through the electron temperature dependence.

In summary, we have experimentally demonstrated finite $\bar{n}R/B_t$ values at $1/q_a = 0$ in the Murakami–Hugill diagram for AC operation in the case of an optimally applied vertical equilibrium field and a horizontal compensation field. If the current rampdown phase is carefully controlled, as in this experiment, even in normal pulsed tokamak operation the $\bar{n}R/B_t$ value may become finite rather than zero at the limit $1/q_a = 0$ because of a finite particle confinement time. Gas puffing before the current reversal has been shown to produce higher

current AC operation and improved reproducibility. On the basis of the observed $\bar{n}R/B_t$ value at $1/q_a = 0$, we can roughly estimate the plasma density at the current reversal for AC operation in a future tokamak reactor. We have given a qualitative explanation for the finite plasma density at the current reversal on the basis of a simple parallel resistance circuit model with a short-circuit effect due to the limiter.

During the preparation of this paper, successful AC operation in JET has been reported [17, 18]. Although the dwell time in JET is still finite (50 ms) and not zero as in the STOR-1M tokamak, this work has demonstrated the possibility of using the AC scheme as an efficient current drive in a future fusion reactor instead of non-inductive current drive [1, 2].

ACKNOWLEDGEMENTS

The authors thank Dr. S.W. Wolfe, Mr. J. Ratzlaff, Mr. A. Witmans, Dr. M. Emaami, Dr. A. Sarkissian, Mr. D. McColl, Dr. W. Zhang and Mr. K.C. Mark for technical assistance. One of the authors (O.M.) is grateful to all faculty members in the Department of Electrical Engineering in the Kumamoto Institute of Technology for encouragement; he also wishes to thank the Japan Society for the Promotion of Science and the NSERC Canada for supporting his stay in Saskatoon during the summer of 1991.

REFERENCES

[1] MITARAI, O., WOLFE, S.W., HIROSE, A., SKARSGARD, H.M., in Plasma Science (Proc. IEEE Int. Conf. Saskatoon, 1986), Institute of Electrical and Electronics Engineers, New York (1986) 39; Fusion Technol. **15** (1989) 204.

[2] MITARAI, O., HIROSE, A., SKARSGARD, H.M., Fusion Technol. **20** (1991) 285.

[3] MITARAI, O., WOLFE, S.W., HIROSE, A., SKARSGARD, H.M., Bull. Am. Phys. Soc. **29** (1984) 1337; Nucl. Fusion **27** (1987) 604.

[4] MURAKAMI, M., CALLEN, J.D., BERRY, L.A., Nucl. Fusion **16** (1976) 347.

[5] AXON, K.B., CLARK, W.H.M., CORDEY, J.G., et al., in Plasma Physics and Controlled Nuclear Fusion Research 1980 (Proc. 8th Int. Conf. Brussels, 1980), Vol. 1, IAEA, Vienna (1981) 413.

[6] MITARAI, O., WOLFE, S.W., HIROSE, A., SKARSGARD, H.M., Plasma Phys. Control. Fusion **27** (1985) 395.

[7] KUWAHARA, H., MITARAI, O., VAN HEESCH, E.J.M., et al., in Plasma Physics and Controlled Nuclear Fusion Research 1986 (Proc. 11th Int. Conf. Kyoto, 1986), Vol. 1, IAEA, Vienna (1987) 413.

[8] MUKHOVATOV, V.S., SHAFRANOV, V.D., Nucl. Fusion **11** (1971) 605.

[9] PENG, Y.-K.M., BOROWSKI, S.K., KAMMASH, T., Nucl. Fusion **18** (1978) 1489.

[10] WONG, K.L., ONO, M., WURDEN, G.A., Rev. Sci. Instrum. **53** (1982) 409.

[11] YOSHIKAWA, S., HARRIES, W.L., SINCLAIR, R.M., Phys. Fluids **6** (1963) 1506.

[12] ELTON, R.C., in Plasma Physics, Vol. 9, Part 1, Academic Press, New York (1970) 115.

[13] MITARAI, O., CONWAY, G., HIROSE, A., et al., Experiments on the current rampdown phase in the STOR-M tokamaks, in preparation.

[14] OLSON, O.D., SKARSGARD, H.M., Can. J. Phys. **43** (1965) 855.

[15] GOLANT, V.E., DANILOV, O.B., ZHILINSKII, A.P., Sov. Phys. — Tech. Phys. **8** (1964) 778.

[16] GOLANT, V.E., ZHILINSKII, A.P., SAKHAROV, I.E., Fundamentals of Plasma Physics, Wiley, New York (1980).

[17] HUART, M., BENFATTO, I., CHIRON, D., et al., in Fusion Engineering (Proc. 14th IEEE Symp. San Diego, CA, 1991), Vol. 1, IEEE, New York (1992) 181.

[18] TUBBING, B.J.D., GOTTARDI, N.A.C., GREEN, B.J., et al., Nucl. Fusion **32** (1992) 967.

(Manuscript received 10 February 1992
Final manuscript received 29 June 1992)